

OSCILLATING BLADE DESIGN FOR ENERGY HARVESTING IN AUTONOMOUS SELF-POWERED FLOWMETER

T. Efstathiadis, V. Gkoutzamanis, A. I.Kalfas, A. Kakafikas

Department of Mechanical Engineering,
Laboratory of Fluid Mechanics and Turbomachinery,
Aristotle University of Thessaloniki,
Greece

Keywords: autonomous flowmeter, oscillating blade, self-powered flowmeter

ABSTRACT

This paper presents the development of an energy harvesting mechanism that will power an autonomous flowmeter in the range of milliwatts (mW). More specifically, the power needed to develop a self-powered flowmeter is around 5 mW. The proposed conceptual design consists of a novel blade that has a bluff leading edge and is numerically studied. Energy harvesting is called the process by which small amount of power that otherwise would be wasted as heat, vibration or kinetic energy is captured and used. The proposed shape of the blade leads to the creation of vortices that force the oscillation of the blade. The motion of the blade is a one degree of freedom (1DOF) rotation. At the blade's axis of rotation an electric generator is going to be coupled. This generator is modeled with the use of a damper. The behavior and the performance of the proposed energy harvester is examined with three dimensional, transient, turbulent simulations in the Reynolds number range of $112248 \leq Re_D \leq 1571475$ (using as a characteristic length the pipe's diameter). An investigation of the effect of various parameters on the motion and performance of the energy harvester is being made. So, the effect of the blade's span length, the effect of the flow velocity, the effect of the damper, the effect of the pipe's diameter and finally the effect of using winglets are investigated. Results showed that the effect of the blade's span length is a crucial parameter that can lead to the oscillation or not of the blade while the maximum power that can be extracted is around 50mW for a flow velocity of 2 m/sec inside a pipe of DN200.

NOMENCLATURE

Abbreviations

DOF	Degree of freedom
DFBI	Dynamic Fluid Body Interaction
DAMP	Damping Constant

Symbols

Re	Reynolds Number	
t	Time	[sec]
I	Inertia Moment	[kg·m ²]

r	Radius	[m]
V	Volume	[m ³]
M _p	Pressure Moment	[N·m]
M _t	Shear Stress Moment	[N·m]
M _d	Damper Moment	[N·m]
p	Pressure	[Pa]
τ	Shear Stress	[Pa]
a	Area Vector	
A	Area	[m ²]
v	Velocity	[m/s]
Su	Source or Sink	
T	Viscous Stress Tensor	
f _r	Body force due to rotation	[N]
f _g	Body force due to gravity	[N]
f _u	User defined force	[N]
f _w	Vorticity specific force	[N]
I	Identity Matrix	
k	Turbulent Kinetic Energy	[J/kg]
v _g	Grid Velocity	[m/s]
f _c	Curvature Correction Factor	
G _k	Turbulent Production	
G _b	Turbulent Production buoyancy	
σ _κ	Turbulent Schmidt Number	
Y _m	Dilation Dissipation	
S	Mean strain rate tensor	

Greek symbols

θ	Angle	[rad]
ρ	Density	[kg/m ³]
φ	Transported Scalar Quantity	
μ	Dynamic Viscosity	[kg/m·s]
μ _t	Turbulent Viscosity	[kg/m·s]

INTRODUCTION

The design of dependable measuring devices has always been a parameter of great importance for reliable design and smooth operation of Turbomachinery systems. The main problem of measuring devices is the power supply of these systems; the pursuit is at least for a supply system whose components will not be interfering with the flow, nor will it be easily and quickly exhaustible. This first set of preconditions rather obviously rules out batteries or conventional power systems and directs research towards other solutions. In this

context, the use of a self-oscillating blade was designed in order to capture the wasted kinetic energy of a water flow inside a pipe to provide energy for a device (eg and supply a flowmeter) seems a pretty promising solution if tested; this holds especially if one considers that approximately 5mW would suffice for a self-powered flowmeter. The means through which the energy would be gathered is an energy harvester placed inside the flowmeter (or, better stated, a magmeter). The main idea behind the innovative concept discussed in this paper is to design a novel blade with a bluff leading edge, in order to produce vortices produced by the flow detachment. These vortices will lead to pressure differences around the blade which will create its oscillation. The main parameters that are going to be examined are namely: extracted power, pressure losses, frequency and amplitude of the oscillation and finally, system size. The blade is supposed to rotate around an axis near its leading edge; this represents a structure with one degree of freedom (1 DOF). The final detail to be borne in mind is that a generator will be coupled to the blade to produce power. This electric generator can be modeled with a damper [1] [2]. In what follows, a physical and computational description of the problem is given; the behavior and the performance of the harvester is examined. A number of specific system parameters, such as blade span length, flow velocity, damper, pipe diameter and finally use of winglets is researched and discussed.

An extended body of research is available for the issue of energy harvesting [3], ranging from piezoelectric harvesters [4][5][6] to small-scale bladeless electromagnetic energy harvesters as described by Zhao D. et al [7]. In what follows a review of the most relevant scientific work is presented. Hoffmann D. et al. [8][9] developed an autonomous wireless water meter with a rotational, radial-flux energy harvester. Moreover, an experimental verification of numerical calculations for horizontal axis marine current turbines was made by Bahaj A.S. et al. [10]; the hydrodynamic performance of these turbines was studied too by the same scientific team. Piezoelectric energy harvesting device based on vortex induced vibration has been optimized by [11][12][13]. Allen J. et al. [14] examined performance behavior of energy harvesting “eel” as well as the influence of electrode position in a piezoelectric energy harvesting flag. Zhu Q. et al. [15][16] in a number of works has probed energy harvesting from passive flapping foils, in order to spot the different response regions of the foil motion, together with its energy performance. In this piece of work, the response of a totally passive flapping-foil flow energy harvester in a linear shear flow was reenacted; results provided evidence to the fact that the foil device in this type of flow undergoes a

periodically oscillation, which can be energy-producing. Zhu Q. et al. [17] probes a Joukowski profile; i.e. a spring and a linear damper in the heaving direction, a rotational spring in the pitching direction and a blade. When self-induced oscillation takes place, the foil does a combination of pitching and heaving movements and mechanical energy is extracted from the heaving motion through the damper. In this context, the different responses of system within the parametric space are examined, as well as together with the average power harvesting and the energy harvesting efficiency. A flapping foil energy harvester with an imposed pitching motion was also studied, in which the blade pitching movement is imposed by an actuator and the energy was harvested through the motion in the heaving direction. Moving on to relevant work of other authors Xie Y. et al. [18] investigated energy extraction performance of an oscillating foil with modified flapping motion, whereas Siala F. et al. [19] investigated energy harvesting of a heaving and forward pitching wing with a passively actuated trailing edge. Young J. et al. [20] reviewed several cases of flapping foil power generation and discussed of progress made by different schemas, as well as challenges encountered. Ding L. et al. [21] examined flow induced motion of bluff bodies with different cross sections as well as their energy harvesting performance. The basic concept probed was that as flow passes over the bluff body, Von Karman vortices are created and vortex shedding frequency causes oscillation of the bluff body. As for the piezoelectric energy harvester, it consists of a cylinder, a structural damper, a spring and a harvesting resistance.

PROBLEM PRESENTATION AND DISCUSSION

It is known that when a bluff body is inserted into a fluid, flow separation is taking place around the body and vortices are created downstream. This phenomenon, which was first described by Theodore von Karman, is the cause of motion in the investigated system. This system consists of a blade, with 1 Degree of Freedom (DOF) rotational motion, that will oscillate due to water flow. The oscillation of the blade is an unsteady phenomenon so the simulations that will take place later are unsteady. The term “unsteady” means that the properties for the various points inside the flow field are changing as a function of time. The range of the Reynolds number (using pipe diameter as a characteristic length) is: $112248 \leq Re_D \leq 1571475$ which is above the limit of 4000 (the threshold for turbulent flow), so the 3D simulations will include turbulence models [22]. Also, the range of the Reynolds number (using width of the blade’s leading edge as a characteristic length) is: $2245 \leq Re_L \leq 125718$ a range that can safely be

considered as inside the limits for creation of vortices.

Since the flow inside the pipe is axis-symmetric, there is nothing to excite the movement of a typical blade. So, the idea was to design a blade that will have a bluff leading edge (Fig.1), in order to create detachment of the fluid and vortices, along the lines described in the first paragraph of this chapter.

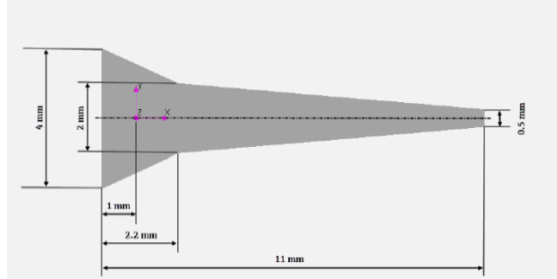


Figure 1: Side view of the novel blade

The existence of the vortices in the velocity field will lead to pressure differences around the blade which in their turn are responsible for the oscillation of the blade, which is placed in the center of the pipe. Energy will be harvested by coupling a generator to the oscillating blade. In order to study the phenomenon already described, simulations will be performed using a commercial computational package. This package can be programmed to incorporate the interaction between the fluid and a free-to-rotate rigid body. To model such a case of fluid body interaction, this software has a module called DFBI (Dynamic Fluid Body Interaction) [23]. Thus, it is possible to simulate the motion of a rigid body in response to the forces the fluid exerts.

COMPUTATIONAL APPROACH OF THE BLADE-PIPE PROBLEM

The problem described in the previous paragraph is a case of fluid - body interaction class of problems, in which the motion of a rigid body inside a water flow is examined. The rigid body is moving because of the fluid forces and moments as show in figure 2.

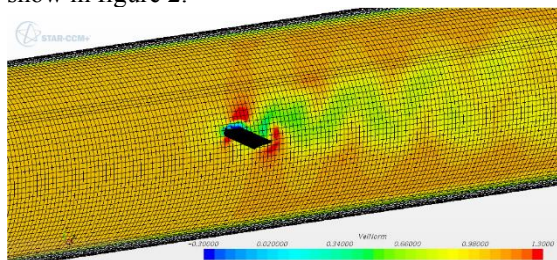


Figure 2: 3D view of the blade into the pipe

So, the governing equation of the motion of the blade is:

$$\sum Moments = (Moment\ of\ Inertia) \cdot \frac{\partial^2 \theta}{\partial t^2} \quad (1)$$

Where:

$\frac{\partial^2 \theta}{\partial t^2}$: the angular acceleration of the rigid blade $\left[\frac{rad}{s^2} \right]$

Moment of Inertia:

$$I = \int (\rho \cdot r^2) dV = \int (\rho \cdot (x^2 + y^2)) dV, [kg \cdot m^2] \quad (2)$$

$\sum Moments$: the moments that applied to the blade.

Those are the Fluid Moments and the Damper Moment. Fluid Moments consist of Pressure Moment and Shear Stress Moment.

Pressure Moment:

$$M_p = \Sigma_f (r_f \times (p_f \cdot a_f)), [N \cdot m] \quad (3)$$

Shear Stresses Moment:

$$M_\tau = -\Sigma_f (r_f \times (\tau_f \cdot a_f)), [N \cdot m] \quad (4)$$

Damper Moment:

$$M_d = -DAMP \cdot \frac{\partial \theta}{\partial t}, [N \cdot m] \quad (5)$$

Where:

DAMP: is damping constant $\left[\frac{N \cdot m \cdot s}{rad} \right]$

$\frac{\partial \theta}{\partial t}$: is the angular velocity $\left[\frac{rad}{s} \right]$

In order for the power transferred to the blade to be calculated, the fluid moments must be multiplied with the angular velocity (in the same way that for the energy harvested to be calculated, the damper moments are multiplied with the angular velocity. So, mean fluid power is equal to mean output power (=mean damper power)

$$\text{Fluid Power} = \text{Fluid Moment} \cdot \text{Angular Vel} \quad (6)$$

$$\text{Output Power} = \text{Damper Moment} \cdot \text{Angular Vel} \quad (7)$$

In the current paper a transient analysis is the most suitable to be employed since there is simultaneously creation of vortices, motion of the blade and turbulent flow inside the pipe; as a result, an implicitly unsteady model with a segregated flow model is used. For turbulence modeling, a K-epsilon model is used together with a 6-DOF solver for blade motion. As already stated, an implicit unsteady model is the recommended approach for vortex shedding, since phenomena of interest are of the same order as diffusion processes. In the implicit unsteady approach, there are some inner iterations between each time-step (in the present case, 5 inner iterations took place) in order to achieve convergence. Acceptable convergence is considered achieved if a decrease of 2 orders of magnitude in the inner iterations in residuals takes place. If a small time-step is used, then a smaller number of inner iteration is required. In the simulations performed for this paper the time-step used depended on flow velocity, since the latter is the parameter defining frequency of blade motion. For the sake of consistency, time-step used is proportional to the flow velocity. To discretize the transient term, a first order scheme was used as follows:

$$\frac{d}{dt}(\rho \cdot \phi \cdot V) = \frac{(\rho \cdot \phi \cdot V)^{n+1} - (\rho \cdot \phi \cdot V)^n}{\Delta t} \quad (8)$$

This scheme is using solution of the current timestep n+1 and solution of the previous time-step n. Moving on to the segregated flow model it solves flow equations (one for each component of velocity and one for pressure) in a segregated manner. With a predictor – corrector approach linkage between the continuity and momentum equation is achieved. The control of the overall solution is done by the SIMPLE algorithm. The general governing equations in continuous integral form are:

Navier - Stokes equation for continuity.

$$\begin{aligned} \frac{\partial}{\partial t} \int_V \rho dV + \oint_A \rho \times (v - v_g) da &= \\ &= \int_V S_u dV \end{aligned} \quad (9)$$

Navier – Stokes equation for momentum:

$$\begin{aligned} \frac{\partial}{\partial t} \int_V \rho v dV + \oint_A \rho v \times (v - v_g) da &= \\ &= - \oint_A P \cdot I da + \oint_A T da + \\ &+ \int_V (f_r + f_g + f_u + f_\omega) dV \end{aligned} \quad (10)$$

Discussing the equations appearing before, the following can be stated: In both equations (continuous and momentum) left-hand side terms are a) the transient term and b) the convective term. In continuity equation on the right side that is a source or a sink (S_u) in our cases is zero. Regarding momentum equation, the pressure gradient can be found on the right-side, together with the viscous force and the body force terms. Water density is taken as 997.561 [kg/m³], dynamic viscosity as 0.00088871 [kg/(m·s)] and the pressure reference is 101325 [Pa]. To model flow turbulence, a K – Epsilon turbulence model is used. A K-Epsilon turbulence model is a two-equation model, in which transport equations are solved for the turbulent kinetic energy (k) and its dissipation rate (ϵ). The transport equations for the Realizable K-Epsilon model are:

$$\begin{aligned} \frac{d}{dt} \int_V (\rho \cdot k) dV + \int_A \rho \cdot k (v - v_g) da &= \\ &= \int_A \left(\mu + \frac{\mu_t}{\sigma_k} \right) \cdot \nabla k da + \end{aligned} \quad (11)$$

$$+ \int_V [f_c \cdot G_k + G_b - \rho \cdot (\epsilon + Y_m)] dV$$

$$\begin{aligned} \frac{d}{dt} \int_V (\rho \cdot \epsilon) dV + \int_A \rho \cdot \epsilon (v - v_g) da &= \\ &= \int_A \left(\mu + \frac{\mu_t}{\sigma_\epsilon} \right) \cdot \nabla \epsilon da + \end{aligned} \quad (12)$$

$$\begin{aligned} + \int_V [f_c \cdot c_{\epsilon 1} \cdot \epsilon + \frac{\epsilon}{k} (c_{\epsilon 1} \cdot c_{\epsilon 3} \cdot G_b) - \\ - \frac{\epsilon}{k + \sqrt{(V \cdot \epsilon)}} \cdot C_{\epsilon 2} \cdot \rho \cdot \epsilon] dV \end{aligned}$$

The turbulent production is evaluated as:

$$\begin{aligned} G_k = \mu_t \cdot S^2 - \frac{2}{3} \rho \cdot k \cdot \nabla v - \\ - \frac{2}{3} \mu_t \cdot \nabla v^2 \end{aligned} \quad (13)$$

The turbulent viscosity is calculated as:

$$\mu_t = \rho \cdot C_m \cdot \frac{k^2}{\epsilon} \quad (14)$$

Where:

$$C_\mu = \frac{1}{A_0 + A_s \cdot U^{(*)} \cdot \frac{k}{\epsilon}} \quad (15)$$

The term $U^{(*)}$ is computed from strain tensor and rotation tensor. All the equations that are related with the K – Epsilon model are solved with the K – Epsilon Solvers (K – Epsilon Turbulence Solver and K – Epsilon Viscosity Solver). The K – Epsilon Turbulence Solver controls the update of the solution of the transported variable k and ϵ . The K – Epsilon Viscosity Solver controls the update of the turbulent viscosity. According to the description of the software's User Guide, the two-layer approach (first suggested by Rodi) is the approach allowing the K – Epsilon model to be applied in the viscous sublayer. By use of this model, the computation is divided to two layers. In the layer next to the pipe wall, the turbulent viscosity μ_t and the turbulent dissipation rate ϵ are functions of wall distance. The values for the dissipation rate for the layer close to the wall are blended smoothly with values calculated from the transport equation for the flow far from the wall. The turbulent kinetic energy k is solved for the entire flow. The two-layer model blends a one-equation model (of Wolfstein in the present case) which solves for turbulent kinetic energy (k) but prescribes algebraically with the distance from the wall the turbulent dissipation rate (ϵ). The turbulent dissipation rate is computed as:

$$\epsilon = \frac{k^{3/2}}{l_\epsilon} \quad (16)$$

The wall treatment that has been used is called «Two layer All y^+ » Wall Treatment is a hybrid approach designed to give similar results with low y^+ treatment when $y^+ \sim 1$ and with high y^+ treatment when $y^+ > 30$. The results are also reasonable even when cell centroid falls in the buffer layer. It also contains a wall boundary condition to be consistent with the two-layer formulation that was briefly described above.

Investigation of the mesh should be done in every CFD problem in order to obtain accurate results. With a good mesh, flow properties can be calculated accurately for every point of the flow field. What is special in the modeling of the conceptual designs, is that there is a rigid body able to move inside the flow. In order to avoid the distortion of the mesh as the blade is moving inside the flow, the software used has a meshing functionality called “Overset Mesh”. With the use of overset mesh, two meshes are created, one that contains the body of interest (in the present case the blade) and one background mesh that contains the surrounding geometry (in our case the water flow into the pipe). Then data is interpolated between the two meshes. This approach allows complex motions to be easily simulated (Fig. 3).

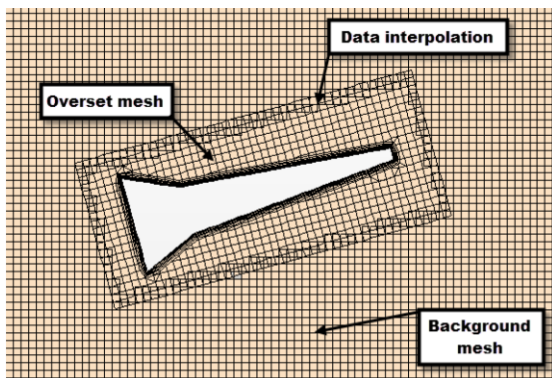


Figure 3: Overset mesh explanation

The rectangular border around the blade (that seems to be denser) is actually where the cells of the overset mesh and background mesh overlap and where the data between the two meshes is interpolated. To obtain more accurate results, the size of the cells of the overset mesh and background mesh that overlap should be the same (if possible). and data is interpolating between them. Of course, treatment and refinement of the mesh takes place around the blade in order to calculate accurately the boundary layer and have Y^+ plus near to one ($Y^+ \approx 1$). Refinement has been done also in broad area around the blade for two reasons in order to capture vortices accurately. The mesh is a predominantly hexahedral mesh, Cartesian, unstructured, with minimal skewness and refinement in the areas of interest (i.e., in the walls of the blade and the area around).

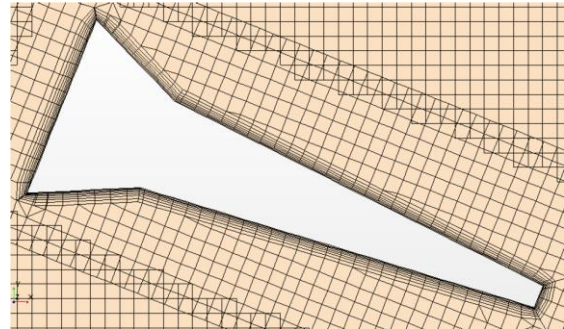


Figure 4: Refinement of the mesh around blade's surface

The computational domain that has been used in all cases has a length of 700 mm. In cases of DN100, the total number of cells is around 2800000 and in cases of DN200, it is around 4300000. The size of the cells in the area of interest around the bodies is 0.28 mm. Of course, refinement has been done around boundaries of the bodies with prism cell layers, in order to capture the boundary layer properly (so the cells are smaller than 0.28 mm in the walls). In figure 5, one can see that most of the cells around the blade surface have $y^+ < 1$ meaning that the boundary layer can be accurately captured.

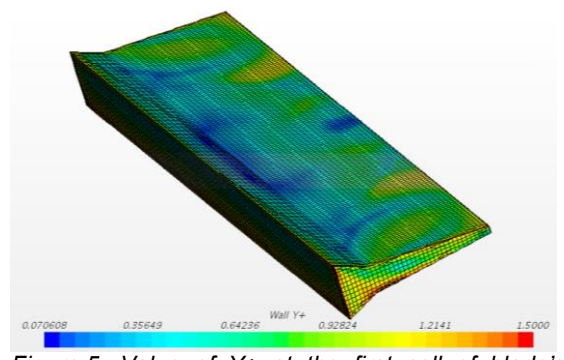


Figure 5: Value of Y^+ at the first cell of blade's surface

Time Step. The selection of an appropriate time step is critical. The size of the time step is the parameter that determines the ability to monitor the phenomenon properly and also of vital importance for the duration of the simulations. In the present case, the time step should be sufficiently small to properly monitor the oscillation of the blade. The selection of a time step smaller than needed will lead to time-consuming computations without any benefit. The proposed approach to select a suitable time step is the following: the approximate von Karman vortices period is calculated with use of Strouhal number for a cylinder. This period is divided with the desired number of steps ($=20$) for each period; thus, an initial time step is obtained. In CFD (Computational Fluid Dynamics) there is a condition called Courant - Friedrichs - Lewy (CFL). The CFL condition is necessary for the convergence and the accuracy of the results. The

definition of CFL condition for 1D (one dimensional) case is:

$$CFL = \frac{u \cdot \Delta t}{\Delta x} \leq 1 \quad (17)$$

When convective Courant number is 1 the fluid moves by about one cell per time step. For time-accurate simulations, the CFL number should be 1.0 on average in the zone of the interest. As a result, the initial time step is divided with an appropriate factor, in order to obtain a time step satisfying the above statements. The steps are taken for a particular velocity. When the velocity changes, the time step and the total simulation time should also change, in order to assure a consistent procedure. So, the steps for the selection of the time step and the total physical time are:

$$\text{New Time step} = \frac{(\text{Time step}) \cdot (\text{Velocity})}{(\text{New Velocity})} \quad (18)$$

$$\text{New Total time} = \frac{(\text{Total time}) \cdot (\text{Velocity})}{(\text{New Velocity})} \quad (19)$$

The time-step for velocity 2 [m/s] is 7.5e-5 [sec] and the total physical time is such that we can monitor around 10 oscillations of the blade. Below there is an image of the CFL number. It is observed that almost all the cells have a CFL number below one and only a few that have CFL>1 (but still ~1).

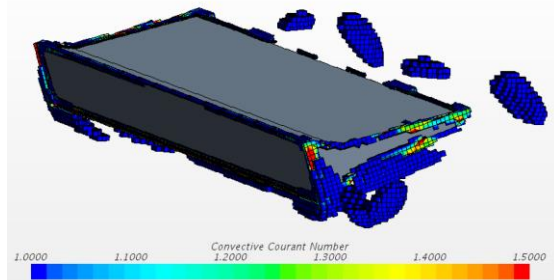


Figure 6: Cells with CFL ≥ 1 around oscillating blade

The time step and total simulation time for the different cases that were selected according to the approach described above are presented hereafter.

DISCUSSION OF STUDIED PARAMETERS

A number of parameters has been probed about the experimental structure described earlier. Results of examination of each important parameter are presented in the next paragraphs. The range of the Reynolds number is: 112248 ≤ Re_D ≤ 1571475. Below there is a table that shows the cases that have been examined.

Table 1. Investigated cases

Velocity [m/s]	Damper [(N*m*s)/rad]	Blade's Span [mm]	Pipe's Diameter [mm]
2	-	10	DN200
2	-	10	DN100
2	1 e-6	50	DN200
2	4 e-6	50	DN200
2	6 e-6	50	DN200
2	12 e-6	50	DN200
2	20 e-6	50	DN200
2	40 e-6	50	DN200
2	4 e-6	50	DN100
2	0.5 e-6	20	DN200
2	1 e-6	20	DN200
2	1 e-6	20(Winglets)	DN200
2	2 e-6	20	DN200
0.5	4 e-6	50	DN200
0.75	4 e-6	50	DN200
1	4 e-6	50	DN200
3	4 e-6	50	DN200
7	4 e-6	50	DN200
0.5	6 e-6	50	DN200
0.5	12 e-6	50	DN200

The normalized velocity field, as the blade oscillates, is shown in the figure 7. One can see the creation of the vortices because of the flow detachment.

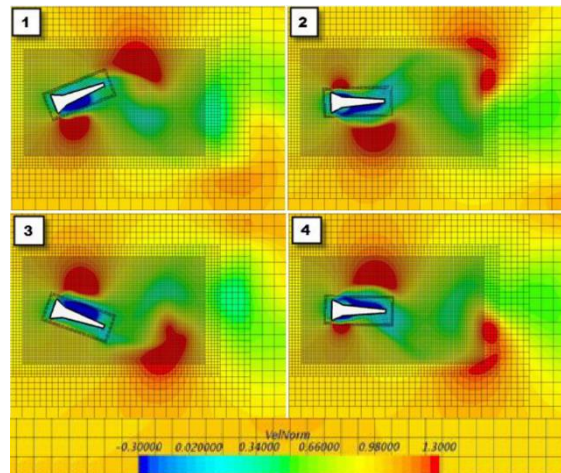


Figure 7: Normalized velocity over ¼ period of oscillation

It is rather obvious by observing 3D simulations and relevant analysis it is proved that the length of the blade span is a crucial parameter of the whole structure. The first reason for postulating about the importance of the blade span length is that by increasing it, the area of the blade is increased; hence, the resulting forces and moment that are applied from the fluid to the blade are increased. The second reason is secondary flows that are created. For smaller span length, vortices created from secondary flows, and, although they are of the same magnitude with secondary flows of the bigger span, they cover bigger area of the blade. As a result, smaller forces are created. Based on the above (and especially on the finding of the secondary flows) can be perceived that there is no oscillation of the blade

for small span length (<20 mm), (in fact there is no motion at all). Also, provided that the optimum damper is used, for a change of the span length from 20[mm] to 50[mm] as shown in the figure 8, the power harvested increases dramatically from 1.4 [mW] to 41.7 [mW].

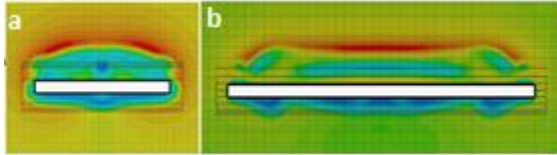


Figure 8: Velocity distribution for a) 20mm and b) 50mm of span

Also, quite obviously, secondary flows cover bigger area of the smaller blade. For a blade with a span length of 10 [mm] no oscillation is observed. Below there is a plot (Fig 9) of the angle of a 10 [mm] blade. It can be seen that the blade finds equilibrium in some angle (around 12 [deg]) and achieves stability (no oscillating). So, no power can be extracted.

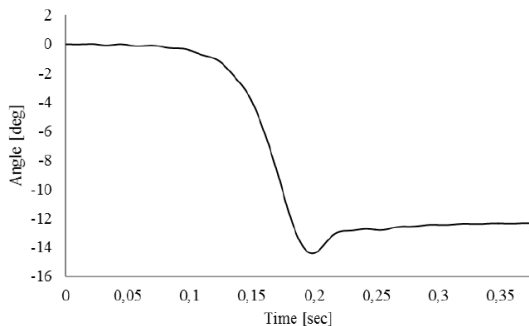


Figure 9: Angle of the blade over time for 10mm span

So, the basic experiment is performed with a blade with span length of 50 [mm] that is placed in the center of a DN200 pipe (≈ 200 [mm]).

RESULTS FOR A BLADE'S SPAN 50[MM], DN200, DAMPER 12E-6[(N·M·S)/RAD]

In the context of this experiment, an oscillating blade is observed. Below, one can see the plot of the angle. Blade motion is monitored for approximately ten periods. The maximum angle of the blade is around 20 [deg], which leads to a maximum vertical displacement of the trailing edge of ± 3.37 mm. The frequency of oscillation is 37.77 Hz. A plot is made for Time > 0.4 sec since it takes a period of time for the blade in order to start oscillating from stationary position.

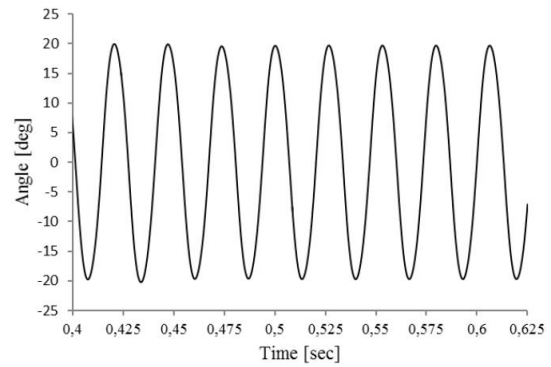


Figure 10: Plot of the angle of the blade over time

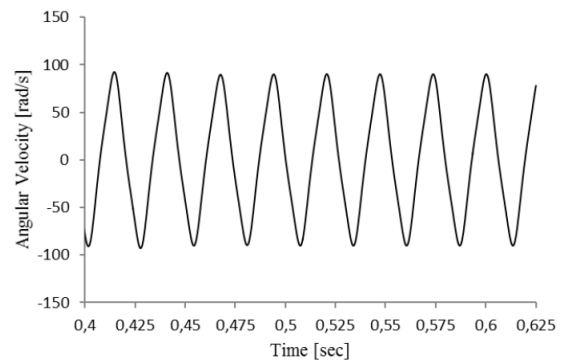


Figure 11: Angular velocity of the blade over time

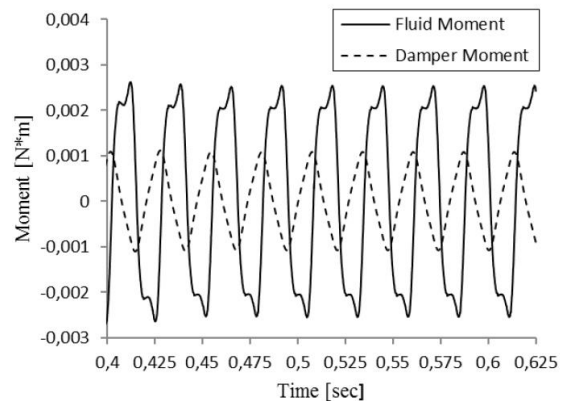


Figure 12: Plots of moments applied to the blade over time

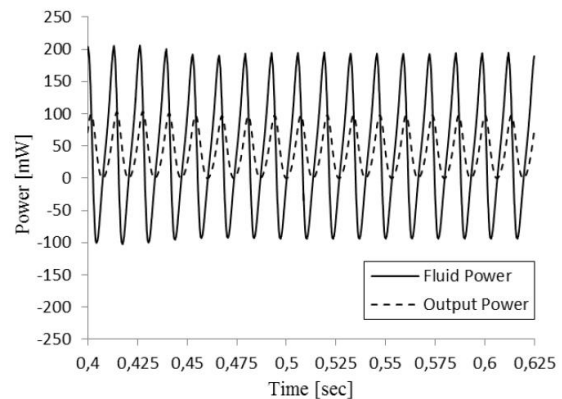


Figure 13: Plot of Fluid Power and Output Power over time

The maximum angular velocity of the blade reaches 90 [rad/s]. The blade's displacement and angular velocity have a 90° phase difference. The blade reaches its maximum velocity when it has minimum displacement and has zero velocity when it has maximum displacement (Fig.11).

The fluid moment and the damper moment are presented in the diagram in figure 12. The moment of the damper is always opposite of the angular velocity of the blade.

In figure 13, one can see that the mean Output Power is around 41.7[mW]. The instant output power is calculated as: Output Power equals to Damper Power which equals to Damper Moment multiplied by Angular Velocity. And the Mean Output Power is the average of the instant output power over time.

The Mean Pressure Drop in this case is around 0.43 [mbar].

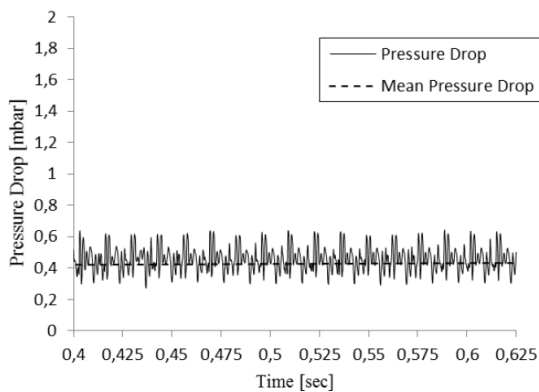


Figure 14: Plot of Pressure Drop over time

Below there are two figures (15,16) showing vorticity near the blade. The first shows the vorticity to a plane perpendicular to the flow and the second shows the vorticity to a plane parallel to the flow.

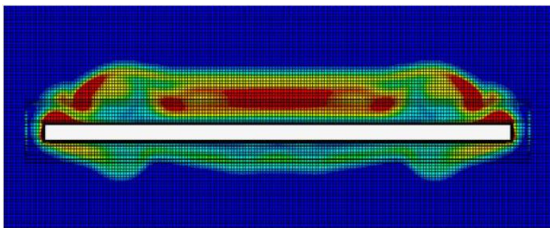


Fig. 15: Vorticity near blade's surface (perpendicular plane)

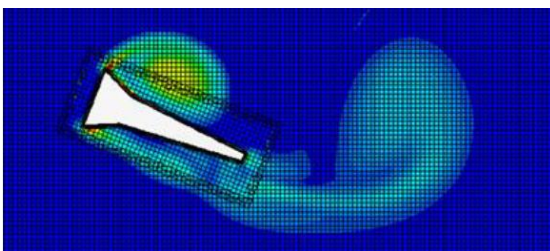


Figure 16: Vorticity near blade's surface (Parallel plane)

• **FLOW VELOCITY**

Effect of flow velocity on the performance of the oscillating blade has been examined in the course of this paper. For a blade of 50 [mm] span, a DN200 pipe and a 4e-6 [(N·m·s)/rad] constant damper, simulations for various flow velocities have been performed, in which the effect of the flow velocity to the maximum angle, the maximum angular velocity, the mean output power etc. are examined. It is observed that, as the flow velocity increases, the maximum angle and the maximum angular velocity of the blade increase also; this finding is expected, since the higher the fluid velocity, the higher the forces that are applied to the blade. Below one can see the figures of the maximum angle and maximum angular velocity and their development over flow velocity. It is observed that the angle of the blade is not a linear function of flow velocity, and the reason for this finding is that as stream flow increases, the frequency of the vortices increases too, which, with its turn, leads to higher frequency and angular velocity of the blade, “restraining”.

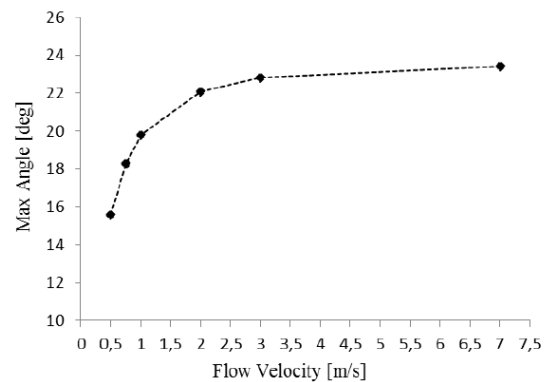


Figure 17: Blade's angle vs flow velocity

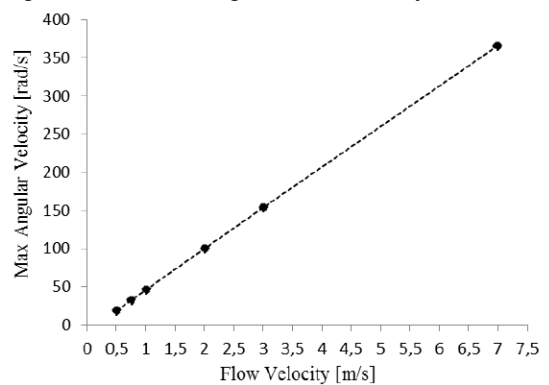


Figure 18: Blade's angular velocity vs flow velocity

The increase of velocity leads to an increase of the mean pressure drop, as well as to steep increase of the mean output power. The increase of the mean power is really high since the power that is carried by the flow is $P = \frac{1}{2} \rho \cdot V^3 \cdot A$. So, the power is a function of the cube of velocity. This is why the plot of the mean output over flow velocity follows this trend.

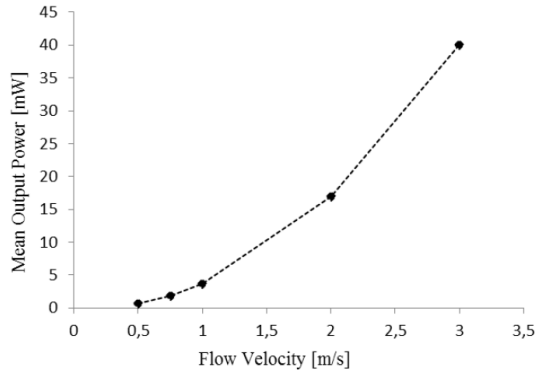


Figure 19: Mean Power Output vs flow velocity

The frequency increases also when velocity increases. The reason is that the Strouhal number should not change with velocity. Since

$$St = \frac{f \cdot d}{V} \quad (20)$$

one can see that if for a constant diameter, velocity increases, then frequency shall increase too, so that the Strouhal number remains the same. As flow velocity increases from 0.5 to 7 [m/s], frequency increases from 10 to 130 [Hz], and the Strouhal number remains almost constant at 0.8.

- **DAMPER**

A research of the effect of the damper to the performance of the oscillating blade has been also performed. For a 50 [mm]-span blade, a DN200 pipe and a constant velocity of 2 [m/s], different dampers have been tested. The effect of the damper to maximum angle, the maximum velocity, the mean pressure drop, the mean output power etc. are examined.

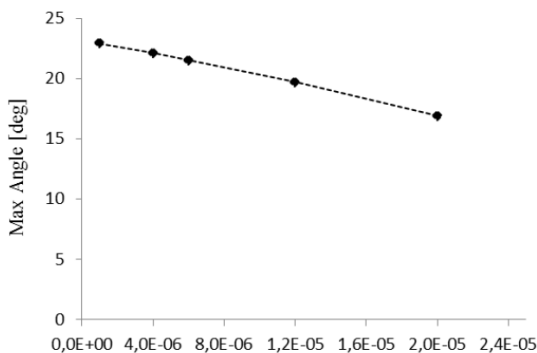


Figure 20: Blade's angle vs damper's constant

As the damper increases the maximum angle of the oscillating blade decreases. That makes absolutely sense, since the higher the damper, the higher the resistance that is applied to the motion of the blade. If the damper increases too much, then the blade cannot overcome the damping and no oscillation takes place. In the particular case, for a

damping constant higher than $20e-6[(N \cdot m \cdot s)/rad]$ the blade again does not oscillate.

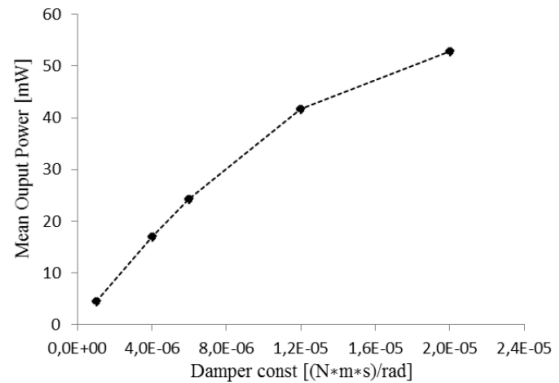


Figure 21: Mean Output Power vs damper's constant

With damper increase, the output power increases too. In this case the optimum (maximum) damper is $20e-6[(N \cdot m \cdot s)/rad]$. For a higher damper, the blade cannot overcome damping and no oscillation takes place.

From all this testing, it is observed that the closer one gets to the optimum damper, the lower the effect of its increase is. When a damper far from optimum is chosen then an increase of the damper causes a really important increase to the Output Power too. For example, the optimum damper for the velocity of 0.5 [m/s] is around $6e-6[(N \cdot m \cdot s)/rad]$. With a higher damper the blade doesn't oscillate. For water velocity 0.5 [m/s], an increase of the damper from $4e-6$ to $6e-6[(N \cdot m \cdot s)/rad]$ leads to a 14.18% power increase. On the other hand, for a water velocity of 2 [m/s] and with the same increase of the damper, leads to a 42.92% power increase. This difference between the two cases comes to an agreement with what was stated before. The opposite holds too: the closer one is to the optimum damper, the smaller the effect its increase has. Further testing for velocity 2 [m/s] it comes out that the increase of the damper leads to a decrease of the maximum angular velocity of the blade. Also, the mean pressure drop slightly decreases, as the damper constant increases, due to the smaller maximum angles.

- **WINGLETS**

A possible means for structure optimization is to embed winglets (as in airplane wings) in order to deter the creation of tip vortices and secondary flows. The blade that was used has a span of 20 [mm].

The increase of the Mean Output Power is around 7.2 %. It is mentioned that the winglets used are not optimized but they have been used just to see the trend of a proposal like that. It seems that the use of winglets can lead to better results.

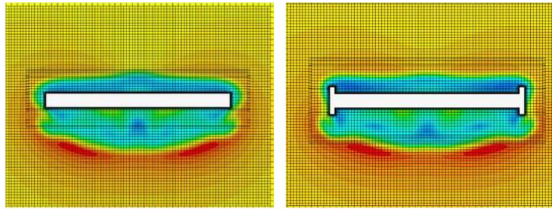


Figure 22: 20mm span blade without and with winglets

• PIPE DIAMETER

The effect of the pipe walls to the performance of the conceptual design of the oscillating blade is also researched. For this purpose, a simulation for DN100 and DN200 pipes has been done. The velocity is taken to be 2 [m/s] and the damper constant equal to $4e-6$. Results prove that there is a slight increase of power produced, from 17 [mW] to 18 [mW], for the smaller pipe diameter. A possible explanation of that may be that walls block vortices, and this leads to increased lift force. Pressure drop (1.65 [mbar]) at the smaller diameter is much higher compared to the 0.47 [mbar] pressure drop that takes place at the DN200 pipe. That is happening as a result of the increased blockage factor (four times higher in the case of DN100 pipe).

CONCLUSIONS

In this paper simulations and feasibility tests for a conceptual design of a novel blade were performed. The grid used for the 3D simulations is Cartesian, unstructured, hexahedral and made up of 4.300.000 cells. Simulations ran at 128 cores and elapsed solver time was approximately 10 hours.

As initially reckoned, energy extracted is heavily depended on flow velocity, since it is proportional to the cube of the velocity. In a numerical application, for a flow velocity of 2 m/s maximum power –to be-extracted reaches 50mW.

Damper is of paramount importance, since this is the decisive parameter for the volume of energy-to-be-extracted (for constant flow velocity and dimension). It was proven that for a given damper and dimensions energy extracted can be measured in the range from 0,65 to 226 mW for a flow velocity of 0,5 to 7 m/sec

Winglets can enhance blade performance and increase extracted energy; therefore, its optimized design (regarding its shape and dimensions) should receive proper diligence.

Furthermore, it should be noted that energy extracted is counted on mechanical terms; therefore, if it is intended to be used for electricity production, a certain efficiency factor must be used. Of course, the path to fully researching electricity production through use of the discussed method of the blade design is not going to be reached effortlessly.

Blade span length is such an important parameter, that in case it is picked to be wrong, no

oscillation will occur. Angle blade varies from 16 deg to 23 deg for velocities ranging from 0,5 to 7 m/s.

REFERENCES

- [1] Zhu, Q.; 2012. “Energy Harvesting by a Purely Passive Flapping Foil from Shear Flows”, *Journal of Fluids and Structures*, v34, October 2012, pp. 157- 169.
- [2] Piñeirua, M.; Doaré, O.; Michelin, S.; 2015. “Influence and optimization of the electrodes position in a piezoelectric energy harvesting flag”, *Journal of Sound and Vibration*, v346, March 2015, pp. 200 – 215.
- [3] Wang, D. A.; Pham, H. T.; Chao, C. W.; Chen, J. M.; 2011. “A Piezoelectric Energy Harvester Based on Pressure Fluctuations in Kármán Vortex Street”, *World Renewable Energy Congress 2011, Sweden*, 8 – 13 May 2011.
- [4] Anton, S. R.; Sodano, H. A.; 2007. “A review of power harvesting using piezoelectric materials (2003 - 2006)”, *Smart Materials and Structures*, v16, 18 May 2007, pp. R1 – R21
- [5] Shan, X.; Song, R.; Liu, B.; Xie, T.; 2015. “Novel energy harvesting: A macro fiber composite piezoelectric energy harvester in the water vortex”, *Ceramics International*, In press.
- [6] Demori, M.; Ferrari, M.; Ferrari, V.; Farisè, S.; Poesio, P.o; 2014. “Energy Harvesting from Von Karman Vortices in Airflow for Autonomous Sensors”, *Journal of Procedia Engineering*, v87, pp. 775-778.
- [7] Zhao, D.; Ji, C.; Teo, C.; Li, S.; 2014. “Performance of small-scale bladeless electromagnetic energy harvesters driven by water or air”, *Journal of Energy*, v74, September 2014, pp. 99- 108.
- [8] Hoffmann, D.; Willmann, A.; Göpfert, R.; Becker, P.; Folkmer B. and Manoli Y.; 2013. “Energy Harvesting from Fluid Flow in Water Pipelines for Smart Metering Applications”, *Journal of Physics, Conference Series* 476 (2013).
- [9] Becker, P.; Folkmer, B.; Göpfert, R.; Hoffmann, D.; Willmann, A. and Manoli, Y.; 2013. “Energy Autonomous Wireless Water Meter with Integrated Turbine Driven Energy Harvester”, *Journal of Physics, Conference Series* 476 (2013).
- [10] Bahaj, A. S.; Batten, W. M. J.; McCann, G.; 2007. “Experimental verifications of numerical predictions for the hydrodynamic performance of horizontal axis marine current turbines”, *Renewable Energy*, v32, October 2007, pp. 2479 – 2490.

- [11]Wen, Q.; Schulze, R.; Billep, D.; Otto, T.; Gessner, T.; 2014. “Modeling and Optimization of a Vortex Induced Vibration Fluid Kinetic Energy Harvester”, *Journal of Procedia Engineering*, v87, pp. 779 – 782.
- [12]He, X. F.; Gao, J.; 2013. “Wind energy harvesting based on flow-induced-vibration and impact”, *Journal of Microelectronic Engineering*, v111, February 2013, pp. 82- 86.
- [13]Blevins, R. D.; 1990. “Flow Induced Vibration”, 2nd Edn., Van Nostrand Reinhold Co.
- [14]Allen, J. J.; Smits, A. J.; 2000. “Energy Harvesting Eel”, *Journal of Fluids and Structures*, v15, pp. 1-12
- [15]Zhu, Q.; 2012. “Energy Harvesting by a Purely Passive Flapping Foil from Shear Flows”, *Journal of Fluids and Structures*, v34, October 2012, pp. 157- 169.
- [16]Cho, H.; Zhu, Q.; 2014. “Performance of a flapping foil flow energy harvester in shear flows”, *Journal of Fluids and Structures*, v51, October 2014, pp. 199 – 210..
- [17]Zhu, Q.; Haase, M.; Wu, C. H.; 2008. “Modeling the capacity of a novel flow – energy harvester”, *Journal of Applied Mathematical Modeling*, v33, pp. 2207 – 2217.
- [18]Xie, Y.; Lu, K.; Zhang, D.; 2014. “Investigation on energy extraction performance of an oscillating foil with modified flapping motion”, *Journal of Renewable Energy*, v63, pp. 550 – 557.
- [19]Siala, F.; Liburdy, J. A.; 2015. “Energy harvesting of a heaving and forward pitching wing with a passively actuated trailing edge”, *Journal of Fluids and Structures*, v57 , May 2015, pp. 1 – 14.
- [20]Young, J.; Lai, J. C. S.; Platzer, M. F.; 2014. “A review of progress and challenges in flapping foil power generation”, *Journal of Progress in Aerospace Sciences*, v67, January 2014, pp. 2 – 28.
- [21]Ding, L.; Zhang, L.; Wu, C.; Mao, X.; Jiang, D.; 2014. “Flow induced motion and energy harvesting of bluff bodies with deferent cross sections”, *Energy Conversion and Management* 91, 2015, pp. 416 – 426
- [22]Holman, J. P.; 2002.. “Heat Transfer”, McGraw-Hill. pp. 207.
- [23]Guide of STAR-CCM+